Research Square

Preprints are preliminary reports that have not undergone peer review.
They should not be considered conclusive, used to inform clinical practice,
or referenced by the media as validated information.

Acid-Activated Jordanian Kaolinite for Efficient Olive Mill Wastewater Treatment: Adsorption of Phenolic Compounds, Heavy Metal Removal, and Mechanistic Insights

Ethar M. Al-Essa
Isra University
Khansaa Al-Essa
k.essa@jpu.edu.jo

Jerash University
Ghayah M. Alsulaim
King Faisal University
Suhad Aleassa
Queen's University Belfast

Research Article

Keywords: Acid-Activated Jordanian Kaolinite, Olive Mill Wastewater, Total Phenolic Compounds, Heavy Metal Ions, Batch and Column Adsorption

Posted Date: September 7th, 2026

DOI: https://doi.org/10.21203/rs.3.rs-10454802/v1

License: This work is licensed under a Creative Commons Attribution 4.0 International License.
Read Full License

Additional Declarations: No competing interests reported.

Abstract

In the Mediterranean region, olive mill wastewater, with its high concentrations of phenolic compounds, dissolved salts, organic matter, and heavy metal ions, is among the most significant agricultural and industrial wastes requiring treatment. Given the well- known high adsorption capacity and low cost of natural Jordanian kaolinite, this study aimed to investigate the effects of acid activation on the adsorption efficiency of Jordanian kaolinite (PK- HCl) for phenolic compounds and the removal of zinc, iron, and manganese ions from olive mill wastewater. Natural kaolinite (PK) was initially purified and then chemically activated using hydrochloric acid. FTIR, XRD, TGA, and BET surface area spectroscopy techniques were employed to study its physical and chemical properties. The results confirmed that acid activation significantly improved structural and surface properties. Adsorption experiments were conducted under various operating conditions, including different adsorbent dosages, temperatures, and initial concentrations of phenolic compounds. The results showed increased adsorption efficiency with higher temperature and adsorbent dosage under the following optimal conditions: 1.0 g of adsorbent, 323 K, pH 6, and a contact time of 4 hours. The removal efficiency of total phenolic compounds reached approximately 54% using PK- HCl, compared to approximately 32% using PK, confirming the endothermic nature of the adsorption process. Additionally, zinc, iron, and manganese ions were removed with high efficiency using PK- HCl. The isothermal adsorption curves exhibited L- type behavior, indicating a strong affinity between the adsorbent and the adsorbate. The equilibrium data also matched the Freundlich and Langmuir isothermal models, indicating that adsorption occurs via a combination of multi- layer adsorption on heterogeneous surfaces and single- layer adsorption on homogeneous active sites. Overall, the results of the adsorption, thermal equilibrium, and analytical tests confirm that acid activation significantly improves the physical, chemical, and adsorption properties of Jordanian kaolinite. Furthermore, the improved, cost- effective, and environmentally friendly PK- HCl adsorbent demonstrates significant potential as an effective material for removing heavy metals and phenolic compounds from olive mill wastewater.

1. Introduction

The Middle East region is presently experiencing a serious water problem as a result of the growing lack of supplies for safe and clean water. Due to the increased rate of industrialization, agriculture and population, water pollution has become a serious issue [1]. Many developing countries of the Middle East have poor wastewater treatment practices that make an urgent need for intervention arise. Despite the fact that current technologies used for treating wastewater continue to evolve, their efficiency in providing water of high enough quality for usage by people and nature is still limited [2]. Therefore, improvement of water safety, availability and resource efficiency has become one of the main goals of sustainable development and prosperity of any country. The fast growth of different industries and agriculture in particular made olive growing the most popular agricultural activity in Mediterranean countries. In Jordan, about 10 million hectares are used for olive planting; there are more than 15 million olive trees and olive oil producing is a large sector of economy [3]. Olive oil manufacturing is associated

with generation of huge amount of wastewater. Olive mill wastewater (OMW), which is the by-product of olive oil manufacturing, is usually discharged to soils and water bodies with no proper treatment.

OMW is a black-brownish, strongly acidic liquid that is considered highly polluted. It is characterized by high concentrations of phenolic compounds, which contribute to its toxicity, elevated organic matter content, significant levels of heavy metal ions, high chemical oxygen demand (COD), and large quantities of total solids [4]. In addition, the large volume of OMW produced (i.e., exceeding 30 million m^3 annually in Mediterranean olive-growing countries) within a relatively short harvesting period further intensifies its environmental impact [5]. OMW (including organic and inorganic pollutants) is therefore one of the most serious sources of agro-industrial pollution in the region. These pollutants pose a hazardous environment to aquatic organisms, aquatic ecosystems, soil quality, groundwater resources, and public health. In particular, the presence of phenolic compounds and their phytotoxicity delays biodegradation and reduces the efficiency of conventional treatment methods. OMW may contain low concentrations of heavy metals (i.e., iron, manganese, copper, zinc, lead, and cadmium). The source of these metals may be agricultural inputs, processing machinery, or natural leaching from the surrounding soil. The presence of both organic pollutants and metal ions further complicates the treatment process. With approximately 780 million people worldwide lacking access to clean and safe drinking water, the development of efficient, low-cost, and sustainable treatment technologies is essential [6].

Solvent extraction, ultrafiltration, evaporation, biological treatment, chemical oxidation, coagulation–flocculation, and reverse osmosis are explored treatment technologies. Despite their potential, many of these methods still present economic and technical challenges, and often simply transfer pollutants from one stage to another without achieving complete removal [7]. They also have limitations, such as high operating and maintenance costs, the generation of secondary pollutants, and sensitivity to high phenol concentrations.

Adsorption technology has become a promising technique for treating OMW due to its simplicity, high efficiency, operational flexibility, scalability, and ability to remove organic and inorganic pollutants. Several natural and synthetic adsorbents have been evaluated for this purpose. This includes activated carbon [8], agricultural wastes [9, 10], bentonite [11], activated bentonite [12, 13], zeolite [14], and clay-based materials [15, 16, 17].

Natural clay minerals (such as kaolinite, bentonite, and zeolite) have garnered significant attention due to their low cost as absorbance, wide availability, chemical stability, environmental compatibility, and distinctive surface properties. Kaolinite is a widespread aluminosilicate mineral characterized by a layered structure, good mechanical strength, and high thermal stability. Jordanian kaolinite deposits represent a valuable local resource that can be utilized for environmental use. However, the adsorption capacity of raw kaolinite is limited by its relatively less surface area, weak surface charge, and limited number of active adsorption sites [18]. Enhancing the adsorption properties of clay minerals is commonly achieved through surface modification techniques. [19, 20]. Among various modification techniques, acid activation is commonly employed to improve surface properties by partially dissolving

octahedral and tetrahedral layers. This process increases porosity, surface area, and the availability of functional groups. Acid-activated kaolinite generally exhibits enhanced surface acidity, improved ion-exchange capacity, and stronger affinity toward organic molecules and metal ions. These characteristics make acid-treated kaolinite a promising, cost-effective, and environmentally sustainable material for wastewater treatment applications.

Recent investigations have highlighted the potential of modified clays as effective adsorbents for eliminating phenolic compounds and heavy metals from water-based systems, although the available research remains limited. [21, 22, 23]. However, comprehensive investigations addressing the simultaneous removal of phenolic pollutants and metal ions from real OMW using locally sourced Jordanian combined with comprehensive physicochemical characterization and adsorption isotherm analysis kaolinite remain limited. Moreover, there is growing interest in exploring new applications of clays, which are natural, abundant, and cost-effective materials. In addition to this, systematic investigations combining physicochemical characterization and modeling of adsorption equilibrium remain quite limited. Combination of these techniques is necessary for understanding the mechanism of adsorption process, estimation of its efficiency, and optimization of purification parameters. This research aims at studying the applicability of Jordanian acid-activated kaolinite as an economical and environmentally friendly adsorbent for the purification of OMW. In order to study the effect of activation on physical and chemical properties of untreated and acid-activated kaolinite, a detailed physicochemical characterization was carried out using different techniques. Adsorption properties of untreated and acid-activated kaolinite towards phenolic compounds and certain metal ions were studied in detail under varying experimental conditions. Modeling of adsorption isotherms provides information about the efficiency and mechanism of adsorption process.

2. Materials and Methods

2.1. Materials

The natural samples of kaolinite were obtained from the area of Al Azraq in eastern Jordan at the coordinates of (31°50'00" N 36°49'00" E). The OMW samples were taken from a centrifuge plant located in the village of Kofranjeh in the province of Jerash (32°17'52.8" N 35°42'14.4" E). Some of the analytical grade reagents used in the experiments are HCl (98%, d = 1.98 g/cm³), silver nitrate ($AgNO_3$) (Puriss) (Merck, Germany), sodium carbonate (Na_2CO_3) (Acros, Belgium), sodium perchlorate ($NaClO_4$) (Simson Pharma Limited, India), and Folin–Ciocalteu reagent and Gallic acid ($C_7H_6O_5$), both sourced from Sigma-Aldrich, Germany.

2.2. Purification of Raw Kaolinite

Natural unprocessed samples of kaolinite were subjected to purification, processing, and refining within the laboratory. Wet sieving through 63μm sieve was done to enhance the purity, whiteness, and to control particle size by eliminating impurities such as quartz, hematite, smectite, mica, illite, carbonates, calcites, and montmorillonite. Moreover, particle size reduction was also done through dispersion and

separation of fine particles from water [24]. Samples were first dispersed in distilled water at 25ºC and stirred using a magnetic stirrer for 10 minutes followed by centrifugation at 800 rpm for 5.0 minutes in order to attain well-dispersed particles. The liquid that contained fine particles was collected in large bottles carefully. This procedure was done five times for each sample to obtain high-purity materials. Suspension was dried at 35ºC on the hot plate. The solids obtained were dried in an oven at 60°C, ground and sieved through a 63 μm sieve [25].

2.3. Activation of Purified Kaolinite by Hydrochloric Acid

A 15 ± 0.01 g of purified kaolinite sample (PK) having particle size below 63 μm was weighted and transferred to the flask. This was followed by adding 200 ml of 1.0 M HCl and stirring it for 24 hours at room temperature. The activated solid was then separated by means of Buchner funnel. The acid-treated kaolinite (PK-HCl) was rinsed multiple times with deionized water until no chloride ions (Cl^{-1}) remained, as verified by the lack of precipitate upon adding 5% $AgNO_3$ solution. The washed material was dried at 100°C for 2 hours and then calcined at 450°C for 4 hours. Once cooled in a desiccator, the activated kaolinite was ground, sieved to smaller than 63 μm, and stored in airtight plastic containers for future use.

2.4. Characterization of Acid-Activated Kaolinite

The activated kaolinite was analyzed through various physicochemical techniques. FTIR spectra were obtained with a Thermo Nicolet NEXUS 670 spectrophotometer. KBr powder, dried at 200°C for 24 hours and ground with kaolinite in a 1:100 ratio using a ball mill, was used. X-ray diffraction (XRD) measurements used a Philips X'Pert Pro diffractometer at 30 kV and 30 mA, with a 1° scatter slit, 0.3 mm receiving slit, a scan rate of 2° per minute, and a sampling pitch of 0.02°. Samples were dried and finely ground before analysis. Thermogravimetric analysis (TGA) was performed with a NETZSCH STA 409 PG/PC thermal analyzer over 0–1000°C at 20°C per minute. The specific surface area was measured using a Gemini VII analyzer (Micromeritics) based on nitrogen adsorption isotherms and the Langmuir method.

2.5. OMW Samples: Collection, Preservation, and Pretreatment

OMW samples were stored at − 2°C in tightly sealed plastic containers and analyzed as needed. For pretreatment, 1 L aliquots of OMW were centrifuged at 10,000 rpm for 30 minutes and then double filtered. The obtained brown-colored solution was served for further analysis.

2.6. Characterization of the OMW

OMW was characterized. Crison PL-700AL meter was used to measure pH, electrical conductivity (EC), dissolved oxygen (DO), oxidation reduction potential (ORP), total dissolved solids (TDS), and salinity. A multi-parameter benchmeter (model PNHI83099-02) was used to determine chemical oxygen demand (COD), alkalinity, total nitrate, total phosphate, and total chlorine levels. Total phenolic compounds (TPCs) were determined using a UV-Vis spectrophotometer (Varian Cary 100) according to the Follin-

Cioalto method. Briefly, 2.5 mL of 0.2 M Follin-Cioalto reagent was mixed with 0.5 mL of the sample, and the sample was incubated in the dark for 5 minutes. Afterward, 2 mL of sodium carbonate solution (i.e., 75 g/L) was added to the sample, and it was incubated again in the dark for one hour. The absorbance was measured at 765 nm, and the TPCs levels were calculated in gallic acid equivalents (g gallic acid equivalents/L) using Beer-Lambert's law. Potassium and sodium determinations were carried out by a Corning 400 flame spectrometer. In the case of heavy metal determination, Zn, Fe, and Mn standards were made in a $NaClO_4$ solution with pH 6 using 0.1 M HCl or NaOH to adjust the pH. The metal ions were determined by an atomic absorption spectrometer Varian Spectra AA-250.

2.7. Adsorption Experiments

2.7.1. Batch Adsorption Experiments for TPCs Removal

Batch adsorption experiments were done to study the efficiency of TPCs removal of PK and PK-HCl. In all the adsorption studies, pH 6 was used, which is lower than the pKa of phenol (9.92) [26], At this pH, phenolic compounds remain undissociated, thereby favoring adsorption. In each experiment, 10 mL of OMW with a certain mass of adsorbent was put in an Erlenmeyer flask and stirred continuously at a constant temperature for four hours. Adsorption process was completed, then filtration was done using a 0.45 μm filter paper to separate the adsorbent. Residual TPCs was determined using UV-Visible Spectrophotometer at λmax. All results were replicated in three trials. The influence of adsorbent mass PK and PK-HCl (i.e., 0.1, 0.5, and 1.0 g; with 10 mL of OMW containing 1340.6 mg/L TPCs), temperature (i.e., 293, 303, 313, and 323 K) and initial TPCs concentrations (i.e., 1215.16, 1340.64, 1442.00, and 1563.43 mg/L; using 1.0 g of adsorbent at pH 6 and 303 K for four hours) on the adsorption process were systematically investigated.

2.7.2. Column Adsorption Experiments for Heavy Metal Ions Removal

The adsorption of Zn, Fe, and Mn ions from OMW by PK-HCl was examined in a fixed bed column configuration. A glass column of dimensions 560 mm × 12 mm filled with about 1.00 ± 0.0001 g of adsorbent was used. About 100 mL of OMW was run through the column, and the effluent was collected in ten 10 mL fractions successively. Three trials were conducted, and the average of the three readings was calculated. The adsorption efficiency (q, mg g^{-1}) is calculated using the formula:

$$q = \frac{(C_o - C_e)}{m} * V$$

1

Where C_o and, C_e (mg/ L) are the initial, and equilibrium adsorbate concentrations, respectively. V (L) is the volume of the solution, and m (g) is the mass of the adsorbent. Removal efficiency (%) was calculated using the following formula [24, 25]:

$$\% \text{ of adsorbate removal } = \frac{(C_o - C_e)}{C_o} \text{ x } 100$$

2

These analytical methods made it possible to evaluate the adsorption equilibrium behavior and the overall processing efficiency.

3. Results and discussion

3.1. Characterization of the PK-HCl

3.1.1. FTIR Spectroscopy Analysis

Figure 1 shows the Fourier transform infrared (FTIR) spectra for both PK and PK-HCl. The results for PK show a broad band at 3459 cm^{-1}, indicating the stretching vibration of physically adsorbed water [26]. The peaks at 3698, 3668, 3657, and 3622 cm^{-1} confirm the stretching vibrations of the structural Al–OH groups and the presence of internal and surface hydroxyl groups in the kaolinite lattice [27]. The peak at approximately 1630 cm^{-1} indicates the bending vibration of water molecules adsorbed on the surface. Moreover, a clear band at 1030–1035 cm^{-1}, 912–915 cm^{-1}, 790–800 cm^{-1}, and 750–755 cm^{-1} are related to the stretching of Si-O bonds, vibrations of Al-OH bonds and vibrations of Si-O-Si and Si-O-Al, respectively. This confirms the presence of aluminum in an octahedral coordination within the kaolinite lattice [28, 29]. Furthermore, the appearance of 540 cm^{-1}, 470 cm^{-1}, and 428 cm^{-1} indicates Si–O–Al bending, Si–O–Si bending, and Si–O vibrations, respectively, as these bands are associated with kaolinite lattice vibrations [30]. Following acid activation (PK-HCl), significant spectral changes were observed, including a broadening of the band at 3460 cm^{-1}, indicating an increase in the amount of physically adsorbed water and surface hydroxyl groups [31]. Furthermore, the weak adsorption characteristics disappeared in the 2100–2450 cm^{-1} range, suggesting the removal of surface impurities and weakly associated species [32]. The marked decrease in the intensity of the hydroxyl bands in the 3695–3620 cm^{-1} range also indicates the loss of structural hydroxyl groups due to aluminum removal [33]. Similarly, the Al–OH bending band (i.e., 912 cm^{-1}) decreased significantly or disappeared. This confirms the leaching of Al^{3+} ions from the octahedral layer [34]. The Si–O bond expansion band widens and shifts slightly (i.e., 1020–1040 cm^{-1}). This indicates the formation of a silica-rich amorphous phase [35]. Furthermore, the decrease in signal intensity in the 700–800 cm^{-1} range reflects the disorder of the regular kaolinite structure. However, the band in the 3400–3500 cm^{-1} range indicates the formation of Si–OH group [36]. These newly functional groups would enhance hydrogen bond interactions and improve surface reactivity. Overall, the results obtained of FTIR spectroscopy confirm the success of the dealuminization and surface modification process. This is resulting in a more homogeneous and reactive adsorbent surface, thereby enhancing the adsorption of TPCs.

3.1.2. XRD Spectroscopy Analysis

Figure 2 shows the X-ray diffraction spectra of PK and PK-HCl kaolinite samples. The results are highlighting their crystalline structure before and after acid activation. It is clear to notice the sharp peaks in the diffraction pattern of PK. This indicates a highly crystalline structure. The characteristic reflections at $2\theta \approx 12°$ and 25° correspond to the (001) and (002) planes. This confirms the regular layered structure of kaolinite [37]. Furthermore, the layered structure is partially preserved, and the main kaolinite peaks remain. However, the results show that acid activation led to significant changes in the PK-HCl pattern; including a decrease in peak intensity and a slight widening. These changes indicate a decrease in crystallinity and partial structural disorder resulting from reduced aluminum removal. This could be explained by the leaching of Al^{3+} ions from the octahedral layer which cause structural defects and increase irregularity, thus forming a silica-rich amorphous phase [38]. The absence of new crystalline phases may be due to acid activation primarily inducing structural modification rather than a phase shift. The slight shifts in peak positions may also indicate changes in interlayer spacing and structural rearrangement. These results are consistent with FTIR spectroscopy findings. All above confirm aluminum removal, the formation of additional active sites, enhancing surface accessibility, and facilitating the diffusion and adsorption of TPCs.

3.1.3. Thermogravimetric Analysis (TGA)

The TGA results reveal several distinct mass loss regions that associated with moisture evaporation, dehydroxylation, and thermal decomposition. The initial weight loss was approximately 1.5% below 150°C. This is attributed to the release of physically adsorbed water molecules. A small endothermic peak was observed near 70°C. This corresponds to the removal of weakly bound surface water.

The major weight loss occurred between 400 and 600°C. This is related to the dehydroxylation of kaolinite where structural hydroxyl groups are removed, leading to the transformation of the crystalline structure into metakaolinite. After acid activation, the original PK structure was not completely restored. corresponding to water removal) and 400°C (i.e., corresponding to dihydroxylation).

The lower dehydroxylation loss that consistent with FTIR results indicates partial dealumination and a reduction in the Al–OH content. The dehydroxylation temperature showed only slight changes after acid activation, while the thermal peaks became less intense. This behavior is consistent with the XRD analysis indicating a reduction in the crystallinity of the material. Together, these results demonstrate that acid activation changed the kaolinite structure, resulting in a silica-rich material with enhanced thermal stability. Moreover, the formation of structural defects provided more active sites, which can contribute to better adsorption performance.

3.1.4. BET Surface Area Analysis

The surface area of the adsorbents was studied using BET analysis. The results showed that PK-HCl sample had a higher surface area (i.e., 43.1 m^2/g) than the PK sample (i.e., 33.5 m^2/g). These results suggest the formation of additional porosity and the development of micro and intermediate pore

structures as a result of the removal of aluminum and impurities [39, 40]. The increased surface area is also attributed to the formation of a silica rich amorphous phase. Developing favorable textural properties increases the number of readily available adsorption sites and facilitates the movement of TPCs into the adsorbent's internal pores, thus improving adsorption efficiency. Therefore, the increased surface area directly contributes to improved adsorption performance. These results support the success of acid activation in improving the surface properties of the adsorbent. BET analysis provides strong evidence of the success of the structural modification, and this is consistent with the results of FTIR, XRD, and TGA, as the increase in surface area, development of porosity, and generation of active functional groups indicate an improvement in the adsorption efficiency of PK-HCl.

3.2. Characterization of OMW

Table 1 shows the physical and chemical properties of untreated OMW, consistent with values previously documented in scientific studies. Overall, the results clearly demonstrate that the use of PK and PK-HCl significantly reduced the presence of several pollutants compared to OMW that did not use either kaolinite. Specifically regarding the use of acid activation, the results show that PK-HCl was superior in removing most inorganic contaminants compared to PK. Clearly, it significantly reduced alkalinity by 55% (i.e., 62.5% vs 7.5%). Moreover, total chlorine removal increased by 42.5% (i.e., 84.5% vs 40%). Nitrate and potassium removal also increased by 18.3% and 16.6%, respectively, with PK-HCl compared to PK.

Slight but consistent improvements were observed in the removal of sodium, total dissolved solids, and salts, ranging from 13% to 14% for each. Both treatments resulted in similar reductions (i.e., with PK-HCl vs PK) of phosphates, and chemical oxygen demand (COD) by 9.9%, and 0.2%, respectively. These results indicate that crude kaolinite efficiently absorbs organic loads in OMW and that acid activation significantly enhances its performance with respect to inorganic parameters, particularly alkalinity, chlorine, and nitrates, with a minimal impact on COD removal.

Table 1
Main characteristics of OMW sample; untreated and treated with PK and PK-HCl.

Parameters	Untreated OMW	Literature ranges values	Reference	Treated OMW with PK	Treated OMW with PK-HCl	% Removal PK	% Removal PK-HCl
Sodium (Na^+) ($mg\ L^{-1}$)	297.9	200–570	[41, 42]	195	155	34.5	48.0
Potassium (K^+) ($mg\ L^{-1}$)	6366.3	639–10800	[43, 44]	4155	3100	34.7	51.3
TPCs (g GAE/L)	1.34	0.26–10.7	[45]	1.0	0.91	25.4	32
Alkalinity ($CaCO_3$) ($mg\ L^{-1}$)	2000	3150–9070	[46]	1850	750	7.5	62.5
Total Chlorine ($mg\ L^{-1}$)	20	33.3–142.7	[47]	12	3.5	40.0	82.5
Phosphate (PO_4^{3-}) ($mg\ L^{-1}$)	4120	31.8–1820	[48]	950	640	76.9	84.5
Nitrate (NO_3^--N) ($mg\ L^{-1}$)	360	350–390	[49]	95	29	73.6	91.9
COD ($mg\ L^{-1}$)	12000	1900–220000	[50, 51]	1019	991	91.5	91.7
TDS ($mg\ L^{-1}$)	34700	5900–103200	[52]	17800	13000	48.7	62.5
Salt ($mg\ L^{-1}$)	26700	11900–32000	[53]	13350	9700	50.0	63.7

3.3. Effect of Temperature and Adsorbent dose on the Removal Efficiency of TPCs

To study the effect of adsorption temperature and adsorbent dosage on the adsorption performance of both adsorbents, PK and PK-HCl, four adsorption temperatures (i.e., 293, 303, 313, 323, and 323 K) and three adsorbent dosages (i.e., 0.1, 0.5, and 1.0 g) were investigated. The overall results of Fig. 4 show that by increasing temperature and adsorbent dosage, the TPCs removal efficiency proportionally increased. Additionally, of all the experimental conditions studied, the highest removal efficiency for TPCs (i.e., 54%) was achieved using kaolinite treated with hydrochloric acid at 323 K and a dosage of 1.0 g. Obviously, the results showed a consistently significant difference in the adsorption performance using PK-HCl under all experimental conditions. This is evident at a 0.1 g adsorbent dosage, where the TPCs removal efficiency of the PK-HCl sample increased from 28% to 45% with increasing temperature from 293 K to 323 K, respectively. Meanwhile, the removal efficiency of TPCs in the PK sample increased slightly from 24% to 27% within the same temperature range. Similarly, at a 1.0 g dose, the PK-HCl sample achieved a removal efficiency of approximately 39% at 293 K to 54% at 323 K, while the efficiency of the PK sample was approximately 28% at 293 K to 32% at 323 K. This is attributed to the increased number of available active sites and the expansion of the effective surface area, which facilitates greater adsorption of phenolic compounds. These results confirm that acid activation successfully improves the physicochemical properties of the kaolinite surface. This is supported by the fact that the larger mass of the adsorbent provides more active sites for interaction with total phenolic molecules [54]. Additionally, the marked improvement in adsorption at high temperatures indicates that the adsorption of phenolic compounds is endothermic. The high temperature increases the mobility and diffusion of phenol molecules, facilitating their transfer from the solution to the surface of the adsorbent and then to its porous structure. The increased adsorption efficiency can also be explained by the fact that higher temperatures activate additional adsorption sites and reduce mass transfer resistance [55, 56]. These results support the potential application of PK-HCl as an effective and low-cost sorbent for treating phenol-rich OMW [57, 58, 59].

It is well known that acid activation removes mineral impurities and exchangeable cations from kaolinite. This will increase surface acidity, enlarge pore volume, and generate additional active functional groups such as surface hydroxyl sites. These modifications improve the interaction between phenolic compounds and the adsorbent surface through hydrogen bonding, electrostatic attraction, π–π interactions, and surface complexation mechanisms.

These adsorption results are consistent with the FTIR, XRD, TGA, and BET analyses, which confirm that acid activation modifies the structure of the adsorbent. Specifically, the activation alters surface functional groups, crystallinity, and mineral composition, while increasing porosity, removing impurities, and generating additional active sites—consequently enhancing the overall adsorption performance.

3.4. Adsorption Isotherms

The adsorption behavior of TPCs on PK and PK-HCl was investigated at four temperatures (293, 303, 313, and 323 K). This was to characterize the relationship between equilibrium adsorption capacity (qe (mg/L)) and equilibrium adsorption concentration (Ce (mg/L)) under varying thermal conditions. The

overall results confirm the positive effect of increased temperature on the adsorption capacity of TPCs in both adsorbents. Of all the experimental conditions studied, the highest adsorption capacity was achieved using PK-HCl at 323 K, reaching approximately 55 mg/g. The observed temperature dependence further supports the thermodynamically favorable and endothermic nature of the adsorption process. Additionally, this adsorption capacity was relatively better when using PK-HCl compared to when using PK alone. The results show that the adsorption capacity increased by 66.7% using PK-HCl by increasing the temperature from 293 K (i.e., qe = 33 mg/g) to 323 K (i.e., qe = 55 mg/g). In contrast, the adsorption capacity increased by 12.9% using PK by increasing the temperature from 293 K (i.e., qe = 31 mg/g) to 323 K (i.e., qe = 35 mg/g). Moreover, the obtained adsorption curves exhibit characteristics of an L- type isotherm according to the Giles classification. This indicates a strong affinity between the phenolic compounds and the adsorbent surface at low equilibrium concentrations [60]. Furthermore, the adsorption capacity gradually increased with the increasing of (Ce). This may be explained by as adsorption proceeds without strong competition from the solvent molecules, progressive occupation of the available adsorption sites with decreasing availability of vacant adsorption sites.

This type of isotherm is commonly associated with favorable adsorption processes, where the interactions between the adsorbate and the adsorbent are stronger than those with the solvent. Furthermore, the absence of a steep plateau indicates that complete surface saturation has not been achieved within the studied concentration range, particularly for PK-HCl [61, 62]. The results also show an increase in the adsorption capacity with increasing temperature. This is attributed to improving access to active adsorption sites and enhancing interactions between phenol compounds and the surface of the adsorbent, thus improving adsorption performance. This result indicates that the adsorption process is predominantly endothermic. This means enhancing the kinetic energy and overall mobility of the phenol molecules, reducing the constraints on mass transfer. This, in turn, facilitates their diffusion from the solution to the outer surface and internal pore network of the absorbent material [63].

The PK-HCl adsorption curves show a sharp increase in qe value with increasing equilibrium concentration compared to PK. This indicates a greater affinity for the modified TPCs as an adsorbent. This behavior is attributed to the physicochemical modifications resulting from HCl activation. The observed nonlinear increase in adsorption capacity suggests heterogeneous surface adsorption and the possibility of multiple adsorption layers at higher equilibrium concentrations. The adsorption behavior indicates that PK-HCl has a wider distribution of active sites and stronger interactions between adsorbent molecules compared to PK.

All the results in this study indicate that acid modification significantly improves the adsorption properties of Jordanian kaolinite, increasing its suitability as an effective and economical adsorbent for treating phenol-rich OMW.

The equilibrium adsorption process can be effectively described using the Langmuir and Freundlich models. These models explain the adsorption capacity, surface heterogeneity, and the physical and chemical interactions that facilitate the bond between the adsorbent and the molecule. The Langmuir

model (Eq. 3) is useful for estimating the maximum adsorption capacity. This model generally assumes monolayer adsorption and that a finite number of equally energetic sites are distributed on a uniform adsorbent surface, and that the adsorbed molecules do not interact [24].

$$\frac{C_e}{q_e} = \frac{1}{K_L . q_{max}} + \frac{C_e}{q_{max}}$$

3

where C□ (mg/L) is the equilibrium concentration of TPCs, q□ (mg/g) is the equilibrium adsorption capacity, q□□□ (mg/g) is the maximum monolayer adsorption capacity, and K_L (L/mg) is the Langmuir constant that is related to the affinity between the adsorbent and the adsorbate.

The results (Fig. 6 and Table 2) demonstrate the accuracy of the Langmuir model in describing the adsorption behavior of the TPCs on PK-HC. The appearance of a monolayer on a homogeneous surface and the progressive saturation of the active sites at all studied temperatures support high correlation coefficients ($R^2 > 0.99$). Furthermore, the relatively low values of the Langmuir constant (K_L) indicate a moderate adsorption affinity. The suitability of the adsorption process was further investigated by calculating the separation factor R_L according to Eq. 4.

$$R_L = \frac{1}{1 + K_L . C_o}$$

4

where C_o (mg/L) represents the initial concentration of TPCs. The dimensionless separation factor (R_L) is commonly used to evaluate the favourability of adsorption. It has been reported that values between 0 and 1 indicate favorable adsorption [64, 65, 66]. The calculated R_L values (Fig. 7) ranged from 0.0978 to 0.1224, demonstrating that the adsorption of TPCs onto PK-HCl was highly favorable under the studied conditions. Figure 7 also shows a gradual decrease in the removal rate with increasing TPCs concentration. This is attributed to the limited number of active adsorption sites available on the PK-HCl surface. Clearly, at low initial concentrations, the available adsorption sites are relatively abundant compared to the total number of phenol molecules, resulting in efficient adsorption and high removal efficiency. As the adsorption process continues, the active adsorption sites gradually become occupied until they approach saturation, limiting further adsorption and leading to a decrease in removal efficiency. These results are consistent with previous studies on phenol removal using modified bentonite, which stated that increasing the concentration of the initial adsorbate leads to a decrease in removal efficiency due to the gradual saturation of the available adsorption sites [67].

In contrast to the Langmuir model, the Freundlich model (Eq. 5) assumes surface heterogeneity, considering that adsorption occurs at sites with different energy levels, thus forming multiple layers of the adsorbent material [68].

$$\log q_e = \log K_F + \frac{1}{n}\log C_e$$

5

As shown in Fig. 8, K_F (mg/g) reflects the adsorption capacity of the adsorbent on heterogeneous surfaces. The heterogeneity factor (n, (mg/L)) provides insight into the nature and suitability of the adsorption process. By plotting logq𝕖 versus logC𝕖, the constants K_F and n were determined from the intersection point and slope, respectively. The TPCs adsorption data showed reasonable agreement with the Freundlich model, with a correlation coefficient (R^2) of 0.957. This agreement is further strengthened by the high values of n (i.e., n > 4.848, Table 2). Typically, n values within the range 1 < n < 10 indicate suitable adsorption [69, 70]. Therefore, this result confirms a predominantly physical adsorption mechanism. In addition, the corresponding 1/n values (0 < 1/n < 1) confirm the heterogeneity of the PK-HCl surface and the irregular distribution of adsorption energies [71, 72].

Table 2
Langmuir and Freundlich isotherm constants values for TPCs adsorption on PK-HCl.

Isotherm Model	**Temperature (K)**	**293**	**303**	**313**	**323**
Langmuir	R_L	0.1395	0.1224	0.1066	0.0826
	K_L	0.0051	0.0059	0.0069	0.0091
	q_m	7.8168	8.0201	8.0640	8.8128
Freundlich	n	4.8481	5.2958	5.9604	6.7648
	K_F	1.5774	1.8710	2.2222	2.8905

The overall results show that the L- type adsorption behavior aligns well with both the Langmuir and Freundlich models. The initial sharp increase observed in the L- type curves indicates good agreement with the Langmuir model, confirming a monolayer coverage of relatively homogeneous active sites on the adsorbent surface. This indicates high adsorption affinity and good utilization of available adsorption sites, particularly in the PK-HCl sample. This supports the possibility that phenolic compounds form a more stable adsorption layer on the modified kaolinite surface. Concurrently, the non-ideal plateau shape of the L-type isotherm curves characterized by a lack of complete saturation within the studied concentration range supports the Freundlich model (i.e., the adsorbent surface is heterogeneous and contains adsorption sites with varying energies). This suggests the possibility of multilayer adsorption, especially at high equilibrium concentrations. Furthermore, the more pronounced L- type form and higher adsorption capabilities of PK-HCl compared to PK indicate that the acid modification improved both the surface affinity and the distribution of adsorption sites on the kaolinite surface. The adsorption process likely involves a combination of monolayer adsorption at appropriate energy sites and multilayer

adsorption in heterogeneous regions of the modified surface. The adsorption performance of the PK-HCl sample involves both homogeneous and heterogeneous mechanisms that are temperature-dependent, as illustrated in Figs. 5, 6, and 8. Taken together, these results confirm that acid activation successfully modifies the structural and surface properties of kaolinite (as shown in Figs. 1, 2, and 3), thereby significantly enhancing its ability to adsorb phenolic compounds.

3.5. Adsorption Mechanism and Structure Relationship

The significant physical, chemical, and structural modifications resulting from acid activation enhance kaolinite's adsorption of TPCs. This can be explained by the fact that acid washing removes mineral impurities such as metal oxides (e.g., Fe, Ca, and Mg) and organic contaminants, creating a cleaner surface and improved access to adsorption sites. Additionally, hydrochloric acid partially dissolves the outer layers of kaolinite, producing structural defects and voids within the clay matrix. This promotes the removal of aluminum from the octahedral layer via the leaching of trivalent aluminum ions (Al^{3+}). Consequently, the specific surface area and pore size increase, accompanied by the formation of micro- and meso- pores structures [73]. Furthermore, the adsorption is physical (i.e., Freundlich coefficient $n > 1$), favoring hydrogen bonding between hydroxyl groups of TPC and surface silanol groups, π–π interactions between the aromatic structures of TPC and the siloxane framework, and electrostatic interactions. Additionally, the lower pH imparts a positive charge to the adsorbent surface, attracting the negatively charged phenolic compounds. Furthermore, increased porosity facilitates molecular movement within the pores, thus improving adsorption efficiency [74]. Structure and surface enhancements promote mass transfer and provide additional intraparticle diffusion pathways for TPCs. This increases activity at adsorption sites, particularly the silanol (Si–OH) groups, which protonate acidic conditions to form active ($–OH_2^+$) surface species.

These structural and chemical transformations are strongly supported by physicochemical characterizations: FTIR and XRD confirm dealumination and the formation of active silanol sites within a structurally disordered, silica-rich phase, while TGA and BET validate the framework modifications and the resulting increase in surface area and porosity. Ultimately, all these combined results contribute to high adsorption efficiency and favorable adsorption behavior for PK-HCl.

3.6. Adsorption Behavior and Literature Comparison

Typically, activated clay materials, even after modification, exhibit low to moderate adsorption capacities for phenolic compounds (i.e., $q_{max} < 10$ mg/g) [74, 75]. In this study, as shown in Table 3, the maximum adsorption capacity of PK-HCl is comparable to or exceeds that of several other adsorbent materials (such as surfactant-activated bentonite, Na-bentonite, zinc oxide bentonite, crude bentonite, kaolinite, fuller clay, acid-activated bentonite, thermally activated kaolinite, and crude kaolinite) reported in the scientific literature. This confirms that the use of acids in activating clay materials improves surface functions, porosity, and the density of active sites, thus enhancing adsorption performance.

Table 3
Comparison of the maximum adsorption capacities (q_{max}) value of some natural and activated clays for TPCs removal

Activated Natural Clay	Adsorption Capacity q_{max} (mg/g)	Reference
Surfactant- activated bentonite	5.72	[23]
Na-bentonite	8.76	[75]
ZnO-bentonite	5.23	[76]
Raw bentonite	5.56	
Kaolinite	0.30	[77]
Fuller's earth	0.31	
Bentonite	0.52	
Acid- activated bentonite	4.58	[78]
Thermally activated kaolinite	5.82	[79]
Raw kaolinite	1.71	
PK-NaCl	8.88	[80]
PK-HCl	8.81	This study

3.7. Heavy Metal Ions Removal Using Column Technique

The percentage uptake of Mn, Fe, Zn and ions using PK and PK-HCl under column conditions is presented in Fig. 9. The overall results for all the metal ions studied show that PK-HCl consistently demonstrates superior adsorption performance compared to PK. This confirms that acid activation is effective in improving adsorption efficiency. Moreover, the removal efficiency for Zn ions gradually increased with the number of portions. This indicates the gradual utilization of available adsorption sites along the column. The results, particularly in the initial sections, show that PK-HCl exhibited higher adsorption (96–99.3%) compared to PK (94.5–99%). This suggests improved surface reactivity and accelerated adsorption kinetics due to the increased surface area and active sites. Furthermore, the adsorption efficiency of iron ions increased from 97.4% to 99.9% with an increasing number of sections. The higher performance of PK-HCl compared to PK is due to structural changes caused by acid activation, such as dealumination and the formation of new adsorption sites such as silanol groups, which promote stronger interactions with Fe ions. Additionally, both adsorbents show very high removal efficiencies (> 99%) for all portions for Mn ions, indicating a strong affinity of Mn ions toward kaolinite surfaces. Nevertheless, PK-HCl still shows a slightly higher and more consistent performance, achieving complete removal (~ 100%), highlighting the improved adsorption capacity and stability of the modified material. The obtained results of the adsorption behavior of the studied metal ions could be explained in

the light of the Hard and Soft Acids and Bases (HSAB) theory. The surface of PK-HCl contains an oxygen rich functional group (silanol (Si-OH) and aluminol (Al-OH) groups) that are hard Lewis bases due to electronegative oxygen donor atoms [81, 82]. Accordingly, hard and borderline metal cations such as Mn^{2+}, Fe^{2+} and Zn^{2+} show highly favorable interactions with these oxygen containing adsorption sites [83, 84]. Within the borderline category, these metals can be ranked by their relative hardness based on electron configurations, polarizability, and charge density as follows: $Mn^{2+} > Fe^{2+} > Zn^{2+}$. Consequently, the harder Mn^{2+} ions undergo strong electrostatic attraction and surface complexation with the negatively charged oxygen donor groups, driving its high removal efficiency. In contrast, Fe^{2+} and Zn^{2+}, classified as borderline acids, allowing them to interact efficiently with the heterogeneous oxygenated surface via ion exchange, covalent bonding, and coordination mechanisms. Acid activation enhances these interactions by increasing the density of exposed oxygen-containing functional groups and improving surface accessibility through enhanced porosity and surface area, confirming that adsorption process is heavily controlled by mass transfer and contact time. In addition, the valence and ionic radii of metal ions in solution are the most important factors affecting their relative selectivity [85]. The ionic radius of Mn^{2+} is the largest among the three ions studied, followed by Fe^{2+} and Zn^{2+} with 0.83 Å, 0.78 Å and 0.74 Å, respectively [85, 86]. If the adsorption of metal ions onto PK-HCl is mainly controlled by electrostatic interactions, stronger adsorption of ions with larger ionic radii is expected. Accordingly, the ionic radius order follows: $Mn^{2+} > Fe^{2+} > Zn^{2+}$, which is consistent with the observed selectivity sequence. Moreover, the adsorption efficiency showed an increase with increasing pH up to 6 as a result of decreased competition between protons (H^+) and metal ions for adsorption sites, thus increasing metal adsorption [87, 88]. In acidic environment, there is a competition between protons and metal cations due to excess of protons, but in alkaline environments, precipitation of metal hydroxide could take place in solution, causing interference in the adsorption process and overestimation of the removal efficiency [89]. In addition, adsorbent dose of 1.0 g PK-HCl per 100 mL of OMW has been found to be the most favorable dose for maximum adsorption of all the investigated metal ions. The optimal dosage guarantees adequate number of available sites and efficient utilization of the surface of the adsorbent. The high efficiency of PK-HCl in all experiments carried out confirms that acidification improves the adsorption capacity of adsorbent via surface area enhancement (as proved by BET analysis) and creation of pores along with formation of reactive groups (as proved by FTIR analysis). Collectively, these physicochemical modifications improve the affinity of PK-HCl toward metal ions and promote stronger adsorbate–adsorbent interactions, resulting in enhanced adsorption efficiency under column conditions.

4. Conclusion

In this study, PK-HCl was successfully prepared and evaluated as an efficient and environmentally sustainable adsorbent for the treatment of OMW. Activation by HCl resulted in significant structural and surface modifications, including aluminum removal, decreased crystallinity, increased porosity, increased surface area, and the generation of additional silanol active sites. These findings were confirmed by

physicochemical analyses using FTIR, XRD, TGA, and BET. These modifications produced a more heterogeneous and reactive adsorbent surface with improved adsorption properties.

Batch adsorption results revealed that PK-HCl had higher efficiency in removing the TPCs compared to untreated PK. Increasing the dosage of adsorbent and operating temperature enhanced the removal efficiency showing that the process is an endothermic and favorable process. For the studied conditions, the maximum removal efficiency for TPCs, which was about 54%, was attained under 323 K with 1.0 g of PK-HCl-treated kaolinite. The adsorption isotherm curves exhibited L-type behavior according to the Giles classification, reflecting strong adsorbate–adsorbent affinity and progressive occupation of active adsorption sites. The equilibrium results were well described by both the Langmuir and Freundlich models. In addition, the calculated R_L values ($0 < R_L < 1$) and Freundlich constant ($1 < n < 10$) confirmed that adsorption occurred under favorable conditions. The column experiments demonstrated the near-complete removal of Zn, Fe, and Mn ions from OMW using PK-HCl. These findings indicate that acid activation significantly improves the adsorption performance of Jordanian kaolinite toward both phenolic compounds and metal ions. This study also highlights the strong relationship between structural modification and adsorption behavior, providing valuable insight into the adsorption mechanism and potential large-scale environmental applications of modified clay materials. Overall, the obtained results demonstrate that PK-HCl represents a promising low-cost, locally available, and environmentally friendly adsorbent for the treatment of real-world matrix (OMW) containing both phenolic compounds and metal-contaminated. This capability is particularly important for supporting sustainable agriculture in the Mediterranean region.

Declarations

Author Contribution

All authors reviewed the manuscript

Data Availability

The data that support the findings of this study are available from the corresponding author upon requist.

References

1. Ali I, Aboul-Enein HY. Chiral pollutants: distribution, toxicity and analysis by chromatography and capillary electrophoresis: John Wiley & Sons; 2004.
2. Vilardi G, Stoller M, Verdone N, Di Palma LJCet. Production of nano Zero Valent Iron particles by means of a spinning disk reactor. Chemical engineering transactions. 2017;57:751–6.

3. Al Hiary M, Dhehibi B, Kassam S. Market study and marketing strategy for olive and olive oil sector in the southern arid part of Jordan. Journal of Agricultural Science Technology. 2025;21:1065–77.
4. Al Bawab A, Ghannam N, Abu-Mallouh S, Bozeya A, Abu-Zurayk RA, Al-Ajlouni YA, Alshawawreh Fa, Odeh F, Abu-Dalo MA, Olive mill wastewater treatment in Jordan: A Review. 2018: Publisher.
5. Casa R, D'Annibale A, Pieruccetti F, Stazi SR, Sermanni GG, Cascio BLJC. Reduction of the phenolic components in olive-mill wastewater by an enzymatic treatment and its impact on durum wheat (Triticum durum Desf.) germinability. Chemosphere. 2003;50:959–66.
6. Fairbridge RW, Askew AJ, Herschy R, Herschy R, Herschy R, Hordon RM, Muller RA, Grymes III JM, Fairbridge RW, Herschy R. Water quality for drinking: who guidelines. Encyclopedia of Hydrology and Water Resources: Springer; 2016. p. 706–12.
7. Al-Ajmi F, Al-Marri M, Almomani F, AlNouss AJW. A comprehensive review of advanced treatment technologies for the enhanced reuse of produced water. Water. 2024;16:3306.
8. Ait-Hmane A, Mandi L, Ouazzani N, Ait Hammou H, Hejjaj A, Alahiane S, Assabbane AJD. Combined treatment of olive mill wastewater by multi-soil-layering ecotechnology and adsorption on activated carbon/lime. Desalination Water Treatment. 2021;233:253–60.
9. Al-Essa K, Habib MA, Al-Essa EM. Removal of hexavalent chromium from industrial wastewater using modified imperata cylindrica biosorbent and method validation. Arabian Journal of Chemistry. 2026;19.
10. Abdulaziz N. Amro, Khansaa Al-Essa, Ethar M. Al-Essa, Abbas I.A. Alakhrasd, Mohamed A. Habibd, Taleb Odehf. A study on the ability of processed squeezed bitter almond for the removal of cadmium ions from contaminated water. Desalination and Water Treatment. 2022;276:133–41.
11. Al-Essa K. Olive mill wastewater treatment using a simple raw and purified Jordanian bentonite based low-cost method. Asian Journal of Chemistry. 2018;30:391–7.
12. Al-Essa K, Al-Essa EM. Effective approach of activated Jordanian bentonite by sodium ions for total phenolic compounds removal from olive mill wastewater. Journal of Chemistry. 2021;2021:1–16.
13. Al-Essa K. Activation of Jordanian bentonite by hydrochloric acid and its potential for olive mill wastewater enhanced treatment. Journal of chemistry. 2018;2018.
14. Khasawneh H, Al-Ananzeh NA-A, Al Jarrah A, Hani FFB, Al-Bodour A, Dawagreh A-K. Optimized Zeolite Adsorption for Reducing Organic Load in Olive Mill Wastewater: Kinetics & Isotherm Analyses. Jordanian Journal of Engineering & Chemical Industries. 2025;8.
15. Solomakou N, Kyriakoudi A, Mourtzinos I, Goula AM. Removal of Phenolics From Olive Mill Wastewater Using Activated Spent Coffee Grounds: Toward an Understanding of Adsorption Behavior. Waste and Biomass Valorization. 2025;16:6665–78.
16. Lazaratou CV, Rosoglou J. Table Olive Wastewater Treatment Using the Clay Mineral Palygorskite as Adsorbent. Minerals. 2025;15:861.
17. Abu Shmeis RM, Tarawneh IN, Issa AT. Removal of phenolic compounds from olive mill wastewater using chitosan/kaolinite/iron oxide nanocomposites. Water Science & Technology. 2025;92:1360–78.

18. Al-Essa K, Khalili F. Adsorption of humic acid onto Jordanian kaolinite clay: effects of humic acid concentration, pH, and temperature. Science Journal of Chemistry. 2018;6:1–10.
19. Al-Essa K, Khalili F. Heavy metals adsorption from aqueous solutions onto unmodified and modified Jordanian kaolinite clay: batch and column techniques. American Journal of Applied Chemistry. 2018;6:25–34.
20. Al-Essa K, Khalili F. Sorption of Pb (II) ions by kaolinite modified with humic acids. Journal of Environmental Science and Engineering A. 2016;5:416–31.
21. Mirmohamadsadeghi S, Kaghazchi T, Soleimani M, Asasian N. An efficient method for clay modification and its application for phenol removal from wastewater. Applied Clay Science. 2012;59:8–12.
22. Wang P, Shen X, Qiu S, Zhang L, Ma Y, Liang J. Clay-based materials for heavy metals adsorption: mechanisms, advancements, and future prospects in environmental remediation. Crystals. 2024;14:1046.
23. Cui X, Liao J, Liu H, Tang W, Tie C, Tian S, Li Y. Adsorption of phenols from aqueous solution with a pH-sensitive surfactant-modified bentonite. Separations. 2023;10:523.
24. Yang H, Sun Y, Zhang Q, Pu Y, Wang J, Cao L, Zhou S, Li Q, Qiao C. ZrMOX particles for enhanced removal of methyl orange from wastewater: preparation, characterization, and adsorption study. Adsorption Science Technology. 2022;2022:9685352.
25. Zidane Y, Laouini SE, Bouafia A, Meneceur S, Tedjani ML, Alshareef SA, Almukhlifi HA, Al-Essa K, Al-Essa EM, Rahman MMJFiC. Green synthesis of multifunctional MgO@ AgO/Ag2O nanocomposite for photocatalytic degradation of methylene blue and toluidine blue. Frontiers in Chemistry. 2022;10.
26. Muñoz-García RO, Ruiz-Casillas CA, Lomelí-Rosales DA, Cortés-Ortega JA, Sánchez-Díaz JC, Cruz-Barba LE. A poly (acrylic acid)-based hydrogel crosslinked with hydroxypropylcellulose as a clarifying agent in nickel (II) solutions. Gels. 2025;11:560.
27. Spengler D, Koch-Müller M, Włodek A, Cuthbert SJ, Majka JJE. Hydroxyl in eclogitic garnet, orthopyroxene and oriented inclusion-bearing clinopyroxene, W Norway. EGUsphere. 2024;2024:1–25.
28. de Donato AA, Ghejan B-A, Bakker JM, Bernhardt TM, Bromley ST, Lang SM. Gas-phase production of hydroxylated silicon oxide cluster cations: structure, infrared spectroscopy, and astronomical relevance. ACS Earth and Space Chemistry. 2024;8:1154–64.
29. Yunusov M, Gulomov S, Nasullayev K, Turdiyeva Dk, Isayeva N, Abdurakhmanova Ik, Mustafayev B, Murzin DYJCL. Hydrodesulfurization Catalysts from Aluminium-Containing Waste. Catalysis Letters. 2024;154:4409–21.
30. Ritz M. Infrared and Raman spectroscopy of mullite ceramics synthesized from fly ash and kaolin. Minerals. 2023;13:864.
31. Goudarzi SH, Javanbakht V, Monajemi SA, Mehrabi M. Highly selective and recyclable vanadium–promoted Mg–Sr–Al oxide catalyst for n–butanol ethoxylation. Scientific Reports. 2026.

32. Soe KT, Thansamai S, Thongprong N, Ruengsrisang W, Muhammad IA, Ketsombun E, Supruangnet R, Kaewprajak A, Kumnorkaew P, Saetang V. Simultaneous surface modification and defect passivation on tin oxide–perovskite interfaces using pseudohalide salt of sodium tetrafluoroborate. Solar RRL. 2023;7:2200964.
33. Soliman W, Shahat MA. Chemical activation of kaolin-based clay bricks as a sustainable route to enhanced mechanical and thermophysical properties. Scientific Reports. 2026;16:4720.
34. Ahnin C, Bounab L, Douhri H, Chraka A, Draoui K, Hadri M. Natural and modified clays for wastewater treatment: a review of adsorption of dyes and heavy metals. Environmental Geochemistry Health. 2026;48:270.
35. Krivoshein PK, Volkov DS, Rogova OB, Proskurnin MA. FTIR photoacoustic and ATR spectroscopies of soils with aggregate size fractionation by dry sieving. ACS omega. 2022;7:2177–97.
36. Jabar TA, Alzuhairi MA, Abed MS. Acidic Influence on Geopolymerization: A Thorough Study Using HCl and Iraqi Kaolin. Russian Journal of Applied Chemistry. 2024;97:104–13.
37. Xue H, Dong X, Fan Y, Ma X, Yao S. Study of structural transformation and chemical reactivity of kaolinite-based high ash slime during calcination. Minerals. 2023;13:466.
38. Purbey R, Bora D, Bharadwaj C, Chetia P, Dutta K, Maheswari R U, Jarugala J, Rotimi Sadiku E, Periyar Selvam S. Development of poly (lactic acid) nanocomposite films with kaolin/bentonite blended clay for packaging applications. International Journal of Polymer Analysis Characterization. 2025;30:203–26.
39. Al-Ameri OB, Alzuhairi M, Bailón-García E, Carrasco-Marín F, Amaro-Gahete J. Transforming petrochemical processes: Cutting-edge advances in kaolin catalyst fabrication. Applied Sciences. 2024;14:9080.
40. Liang X, Li Q, Fang Y. Preparation and characterization of modified kaolin by a mechanochemical method. Materials. 2023;16:3099.
41. Eroğlu E, Eroğlu İ, Gündüz U, Yücel M. Effect of clay pretreatment on photofermentative hydrogen production from olive mill wastewater. Bioresource Technology. 2008;99:6799–808.
42. Piperidou CI, Chaidou CI, Stalikas CD, Soulti K, Pilidis GA, Balis C. Bioremediation of olive oil mill wastewater: chemical alterations induced by Azotobacter vinelandii. Journal of Agricultural Food Chemistry. 2000;48:1941–8.
43. Moreno E, Perez J, Ramos-Cormenzana A, Martinez. Antimicrocial effect of waste water from olive oil extraction plants selecting soil bacteria after incubation with diluted waste. 1987.
44. Hanafi F, Sadif N, Assobhei O, Mountadar M. Traitement des margines par électrocoagulation avec des électrodes plates en aluminium. Revue des sciences de l'eau. 2009;22:473–85.
45. Vlyssides AG, Loizides M, Karlis PK. Integrated strategic approach for reusing olive oil extraction by-products. Journal of Cleaner production. 2004;12:603–11.
46. Mouncif M, Tamoh S, Faid M, Achkari-Begdouri A. A study of chemical and microbiological characteristics of olive mill waste water in Morocco. Grasas y Aceites. 1993;44:335–8.

47. Bouknana D, Hammouti B, Salghi R, Jodeh S, Zarrouk A, Warad I, Aouniti A, Sbaa M. Physicochemical characterization of olive oil mill wastewaters in the eastern region of Morocco. J Mater Environ Sci. 2014;5:1039–58.
48. Aly AA, Hasan YN, Al-Farraj AS. Olive mill wastewater treatment using a simple zeolite-based low-cost method. Journal of environmental management. 2014;145:341–8.
49. Panizza M, Cerisola G. Olive mill wastewater treatment by anodic oxidation with parallel plate electrodes. Water research. 2006;40:1179–84.
50. Passarinho P. Olive Mill Wastewater detoxification: PhD Thesis, Instituto Superior Técnico, Universidade Técnica de Lisboa, Portugal; 2002.
51. Mendoza JA. Nuevas tecnologías para la obtención de aceite de oliva. SIDALC. 1994.
52. Hamdi M. Thermoacidic precipitation of darkly coloured polyphenols of olive mill wastewaters. Environmental Technology. 1993;14:495–500.
53. Al-Essa K. NaCl – Activated Jordanian Bentonite for Olive Mill Waste water Treatment: Evaluation of Physicochemical Properties, Adsorption of Phenolic Compounds: Isotherms and Thermodynamic Studies Research Journal of Pharmaceutical, Biological and Chemical Sciences. 2018;9:1362–84.
54. Akhtar MS, Ali S, Zaman WJ. Innovative adsorbents for pollutant removal: exploring the latest research and applications. Molecules. 2024;29:4317.
55. Gupta SS, Bhattacharyya KG. Adsorption of heavy metals on kaolinite and montmorillonite: a review. Physical Chemistry Chemical Physics. 2012;14:6698–723.
56. Hong H, Sun Z, Fu Z, Min XJ. Adsorption of AUCL 4 – by Kaolinites: Effect of pH, Temperature and Kaolinite Crystallinity. Clays clay minerals. 2003;51:493–501.
57. Dou W, Deng Z, Fan J, Lin Q, Wu Y, Ma Y, Li Z. Enhanced adsorption performance of La (III) and Y (III) on kaolinite by oxalic acid intercalation expansion method. Applied Clay Science. 2022;229:106693.
58. Zhang A, Liu J, Yang Y, Yu Y, Wu D. Experimental and theoretical studies on the adsorption performance of lead by thermal pre-activation and phosphate modified kaolin sorbent. Chemical Engineering Journal. 2023;451:138762.
59. Abdalqadir M, Rezaei Gomari S, Pak T, Hughes D, Shwan D. A comparative study of acid-activated non-expandable kaolinite and expandable montmorillonite for their CO2 sequestration capacity. Reaction Kinetics, Mechanisms Catalysis. 2024;137:375–98.
60. Ismail M, Amor HB. Removal of Rhodamine B Dye Using Sustainable Activated Carbon Derived from Date Stones. RHAZES: Green Applied Chemistry. 2026;24:35–45.
61. Gautam, Sah RP, Sahoo S. A review on adsorption isotherms and kinetics of CO2 and various adsorbent pairs suitable for carbon capture and green refrigeration applications. Sādhanā. 2023;48:27.
62. Pei C, Zhang N, Liu Q, Shen J, Huang M, Qian Y, Lv C, Wu T, Yu K, Liu C. Predicting maximum adsorption capacity of antibiotics on biochar: An end-to-end approach based on saturated and unsaturated adsorption isotherms. Agricultural Environment Sustainability. 2025:100004.

63. Das P, Nayak PK, krishnan Kesavan R. Kinetic and thermodynamic characterization of thermosonication-assisted extraction of bioactives from lapsi fruit juice optimized by ANN-GA. Sustainable Food Technology. 2025;3:1624–35.
64. Khater D, Alkhabbas M, Al-Ma'abreh AM. Adsorption of pb, cu, and Ni ions on activated carbon prepared from oak cupules: kinetics and thermodynamics studies. Molecules. 2024;29:2489.
65. Al-Ma'abreh AM, Hmedat DA, Edris G, Hamed MA. Removal of heavy metal ions (Pb2+, Co2+, and Cd2+) by activated carbon from cypress fruit: an investigation of kinetics, thermodynamics, and isotherms. Journal of Chemistry. 2024;2024:1984821.
66. Al-Ma'abreh AM, AlKhabbas M, Alawaideh S, Hussein-Al-Ali SH, Hmedat DA, Edris G, Abuassaf RA, Hamed MA. Investigation of kinetics, thermodynamics, and isotherms of the simultaneous removal of heavy metal ions by activated carbon from cypress fruit. Adsorption Science Technology. 2024;42:02636174241256853.
67. Ahmadi S, Igwegbe C. Adsorptive removal of phenol and aniline by modified bentonite: adsorption isotherm and kinetics study.. Appl Water Sci 8: 170. 2018.
68. Al-Essa K, Al-Essa EM. Effective approach of activated Jordanian bentonite by sodium ions for total phenolic compounds removal from olive mill wastewater. Journal of Chemistry. 2021;2021:7405238.
69. Farhan AM, Al-Dujaili AH, Awwad AM. Equilibrium and kinetic studies of cadmium (II) and lead (II) ions biosorption onto Ficus carcia leaves. International Journal of Industrial Chemistry. 2013;4:24.
70. Malik PK. Use of activated carbons prepared from sawdust and rice-husk for adsorption of acid dyes: a case study of Acid Yellow 36. Dyes pigments. 2003;56:239–49.
71. Goldberg S. Equations and models describing adsorption processes in soils. Chemical processes in soils. 2005;8:489–517.
72. Saad EM, Hassan HM, Soltan MS, Butler IS, Mostafa SI. Removal of copper (II) ions from Aqueous Media by Chemically Modified MCM-41 with N-(3-(trimethoxysilyl) propyl) ethylenediamine and Its 4-hydroxysalicylidene Schiff-base. Environmental progress sustainable energy. 2018;37:746–60.
73. Valtchev V, Tosheva LJCr. Porous nanosized particles: preparation, properties, and applications. Chemical reviews. 2013;113:6734–60.
74. Peng M, Hsu J, Luo J, Huang XJ. Mechanistic insights into dichloromethane adsorption by nitrogen-functionalized biochar. Separation Purification Technology. 2026;393:137251.
75. Asnaoui H, Dehmani Y, Khalis M, Hachem E-K. Adsorption of phenol from aqueous solutions by Na–bentonite: kinetic, equilibrium and thermodynamic studies. International Journal of Environmental Analytical Chemistry. 2022;102:3043–57.
76. Desnelli D, Rizkiani D, Alfarado D, Ferlinahayati F, Yohandini H, Fatma F, Mara A, Suheryanto S, Nurnawati E, Hamidah A. Adsorption study on phenol from bentonite doped with zinc oxide: synthetis, characterization, equilibrium, kinetics, and thermodynamic. IJFAC. 2024;9:82–95.
77. Safwat SM, Medhat M, Abdel-Halim H. Phenol adsorption onto kaolin and fuller's earth: a comparative study with bentonite. Desalination Water Treatment. 2019;155:197–206.

78. Ahmadi S, Igwegbe CA. Adsorptive removal of phenol and aniline by modified bentonite: adsorption isotherm and kinetics study. Applied Water Science. 2018;8:170.
79. Ghogomu JN, Noufame DT, Tamungang EBN, Ajifack DL, Ndi JN, Ketcha JM. Adsorption of phenol from aqueous solutions onto natural and thermally modified kaolinitic materials. Int J Biol Chem Sci. 2014;8:2325–38.
80. Al-Essa EM, Al-Essa K, Halalsheh N, Lagum AA, Al-Ma'abreh AM, Saraireh H, Shatnawi K. Removal of Total Phenolic Compounds and Heavy Metal Ions from Olive Mill Wastewater Using Sodium-Activated Jordanian Kaolinite. Sustainability. 2025;17:4627.
81. Dong-xue H, Yu-chen G, Rong C, Zi-qi M, Biao W. Competitive adsorption mechanism of ball clay in water contaminated by multi-component heavy metal. Environmental Technology Innovation. 2026:104862.
82. Luo X, Wang X, Xia C, Peng J, Wang Y, Tang Y, Gao F. Quantitative ion character-activity relationship methods for assessing the ecotoxicity of soil metal (loid) s to lettuce. Environmental Science and Pollution Research. 2023;30:24521–32.
83. Maneechakr P, Karnjanakom S. Environmental surface chemistries and adsorption behaviors of metal cations (Fe 3+, Fe 2+, Ca 2 + and Zn 2+) on manganese dioxide-modified green biochar. RSC advances. 2019;9:24074–86.
84. Kumar A, Chauhan U, Sesma RK, Rana N, Gathania AK. Plant-derived carbon quantum dots for dual applications in hexavalent chromium sensing and optical thermometry. Materials Research Bulletin. 2026;200:114108.
85. Dudev T, Nikolova V. Determinants of Fe2 + over M2+ (M = Mg, Mn, Zn) selectivity in non-heme iron proteins. Inorganic Chemistry Frontiers. 2016;55:12644–50.
86. Liu X, Wu M, Li C, Yu P, Feng S, Li Y, Zhang Q. Interaction structure and affinity of zwitterionic amino acids with important metal cations (Cd2+, Cu2+, Fe3+, Hg2+, Mn2+, Ni2 + and Zn2+) in aqueous solution: a theoretical study. Molecules. 2022;27:2407.
87. Juang R-S, Shao H-J. Effect of pH on competitive adsorption of Cu (II), Ni (II), and Zn (II) from water onto chitosan beads. Adsorption Science Technology. 2002;8:71–8.
88. Hsu L-C, Liu Y-T, Syu C-H, Huang M-H, Tzou Y-M, Teah HY. Adsorption of tetracycline on Fe (hydr) oxides: effects of pH and metal cation (Cu2+, Zn2 + and Al3+) addition in various molar ratios. Royal Society Open Science. 2018;5:171941.
89. Bakhtiari S, Salari M, Shahrashoub M, Zeidabadinejad A, Sharma G, Sillanpää M. A comprehensive review on green and eco-friendly nano-adsorbents for the removal of heavy metal ions: synthesis, adsorption mechanisms, and applications. Current Pollution Reports. 2024;10:1–39.

Figures

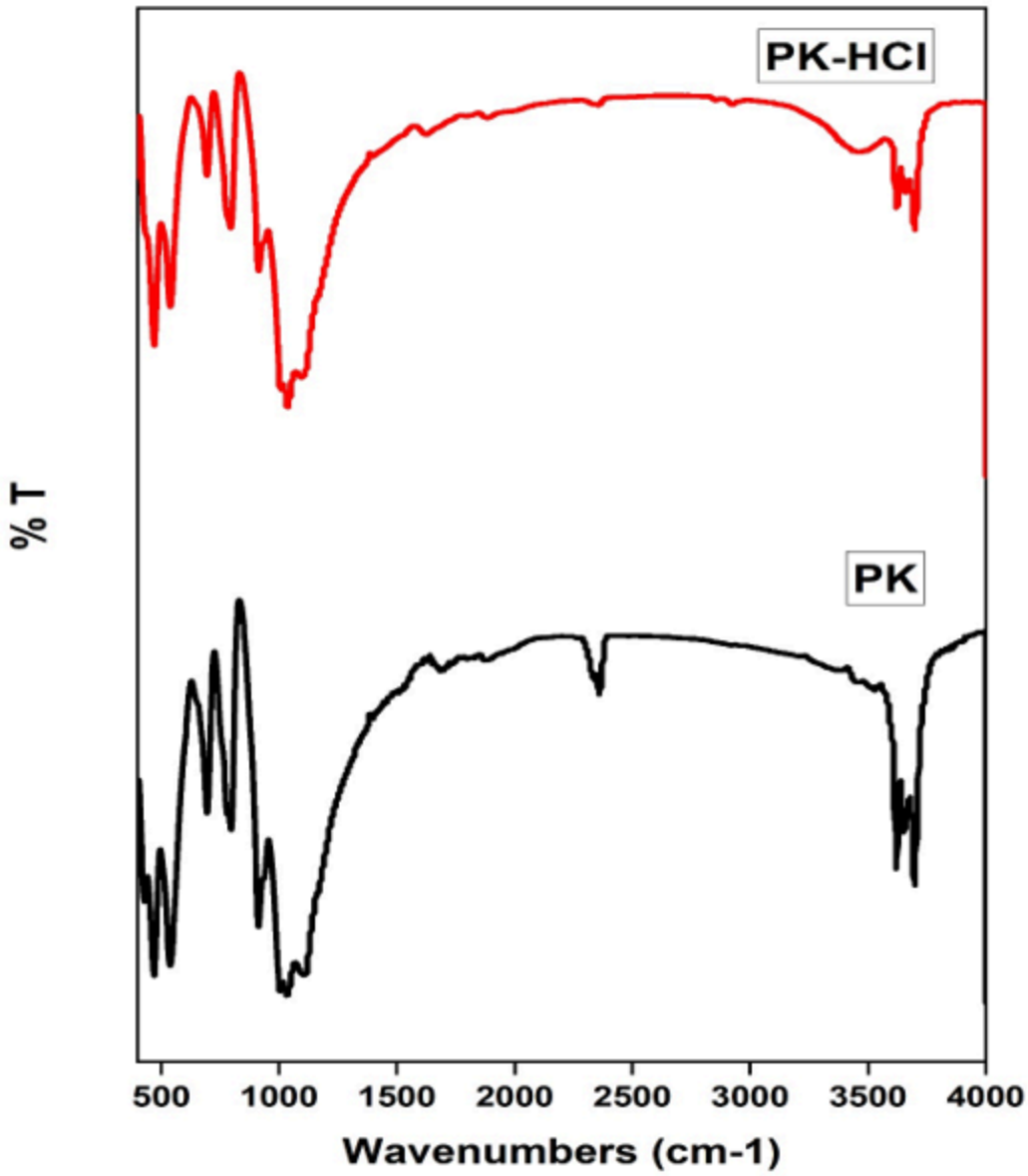


Figure 1

FTIR spectra of PK and PK-HCl adsorbents.

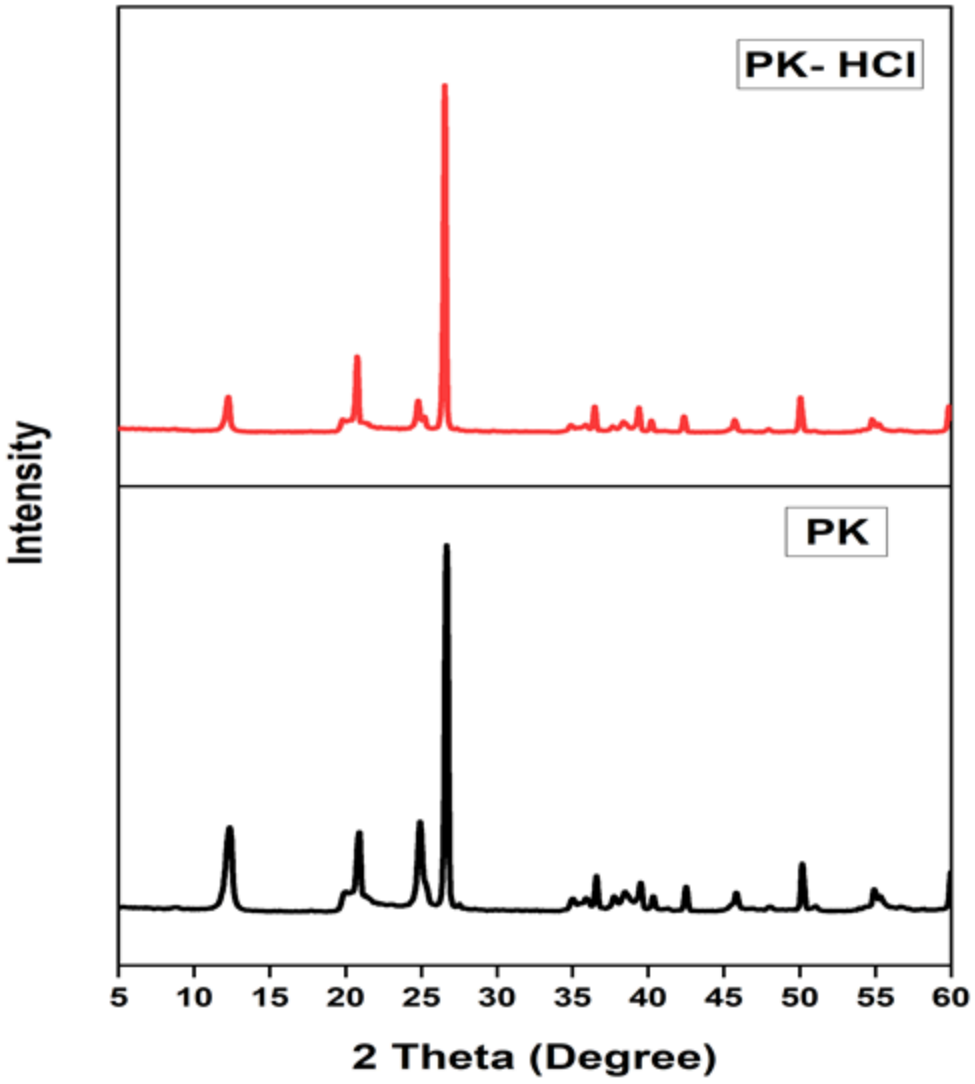


Figure 2

XRD analysis of PK and PK-HCl adsorbents.

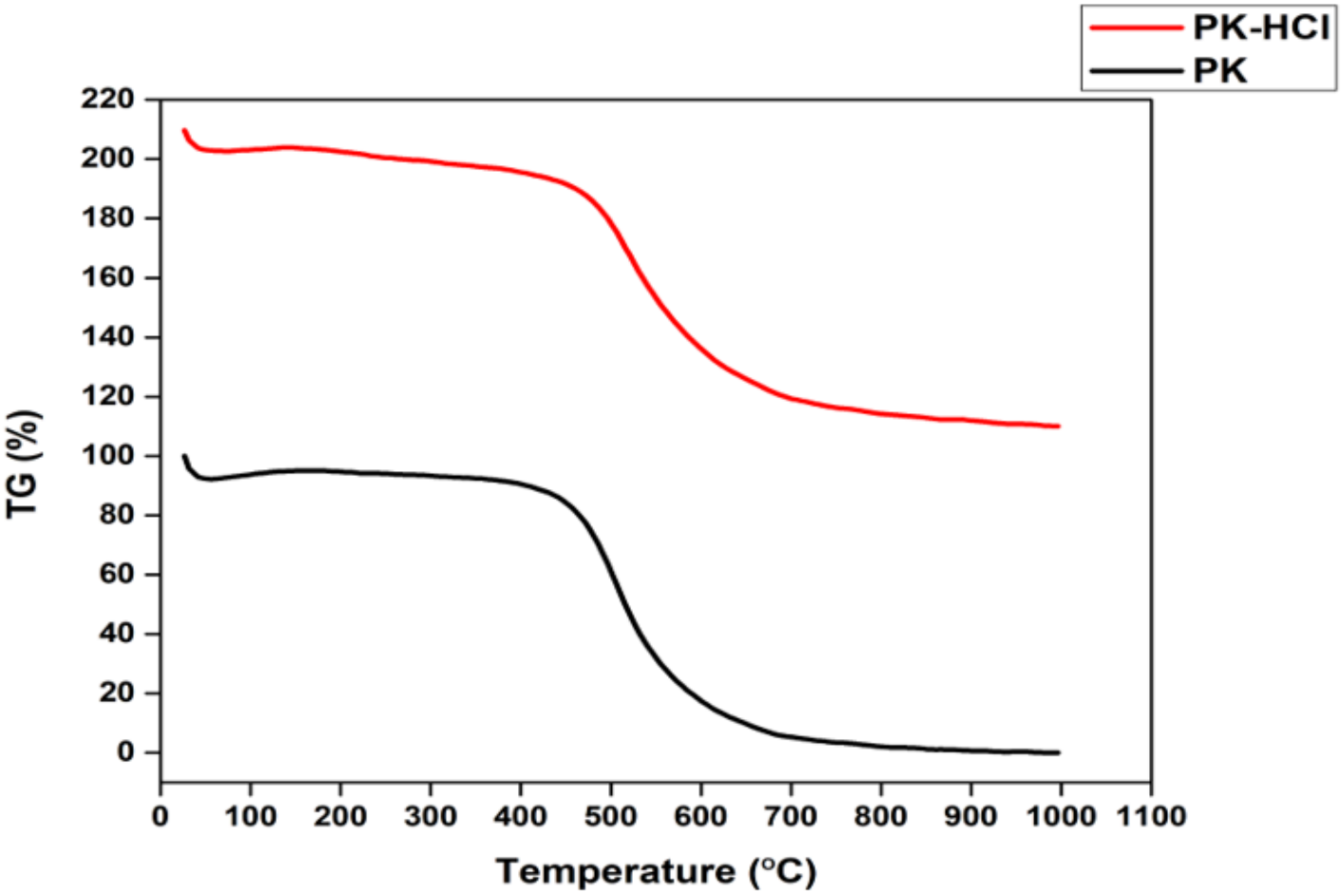


Figure 3

The results of TGA of PK and PK-HCl adsorbents.

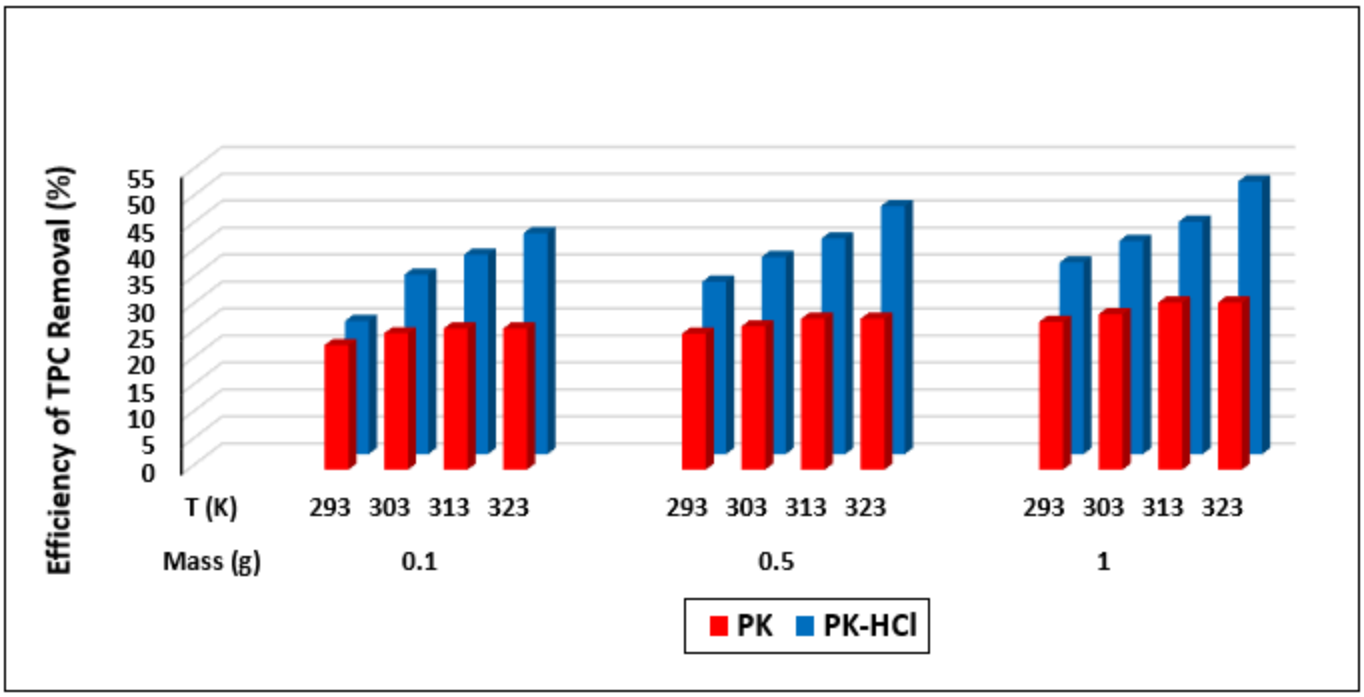


Figure 4

Effect of temperature and adsorbent dose on the removal efficiency of TPCs using PK and PK-HCl. Experimental conditions: initial TPCs concentration = 1340.6 mg/L, adsorbent dose = 0.1, 0.5, and 1.0 g, temperature = 293, 303, 313, and 323 K, 10 mL of OMW, pH =6, and the contact time 4 hours.

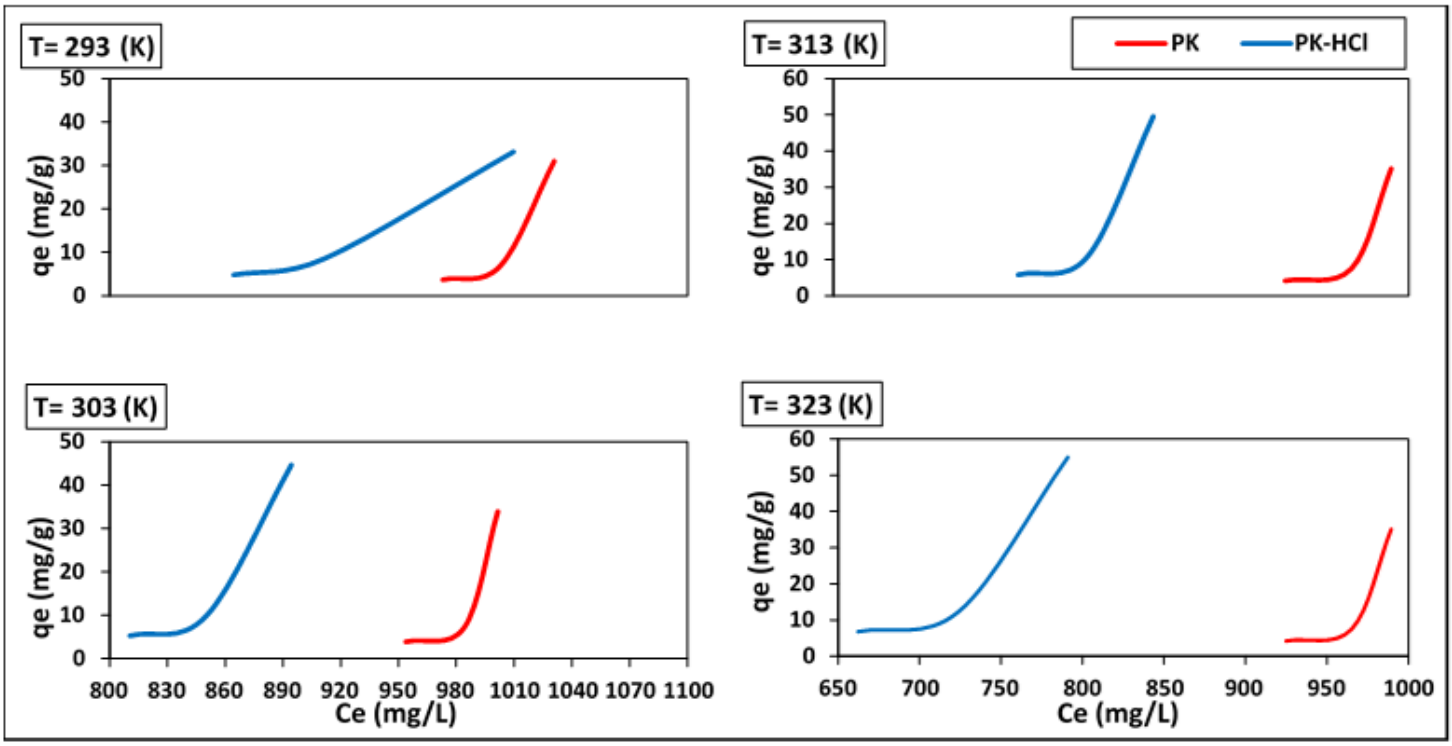


Figure 5

Adsorption isotherm curve of TPCs removal using PK and PK-HCl, effect of temperature and dose. Experimental conditions: initial TPCs concentration = 1340.6 mg/L, adsorbent dose = 1.0 g, temperature = 293, 313, 303, 323 K, 10 mL of OMW, contact time 4 hours, pH=6.

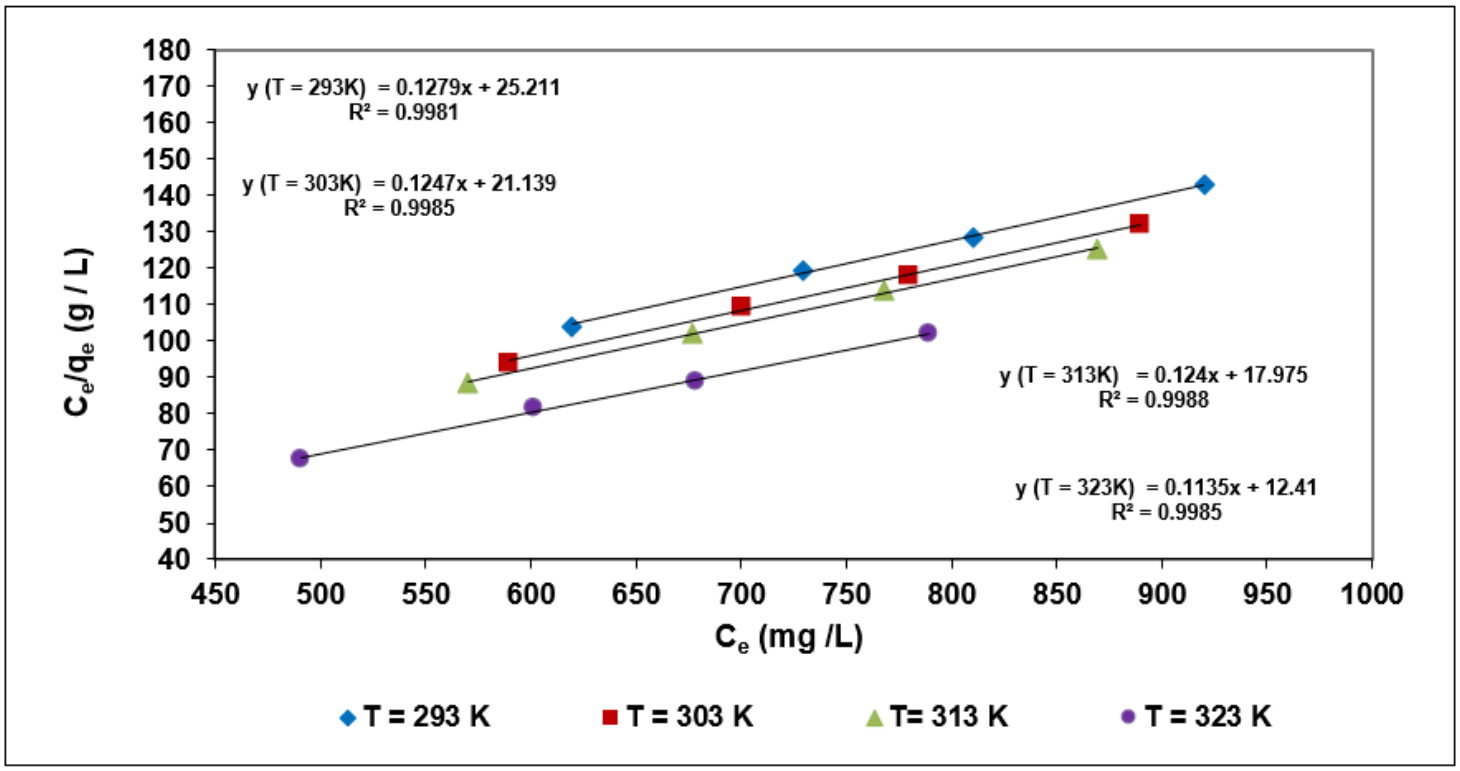


Figure 6

Effect of initial TPCs concentration on the percentage uptake using 1.0 g of PK-HCl, 10 mL of OMW, and constant temperature 303 K.

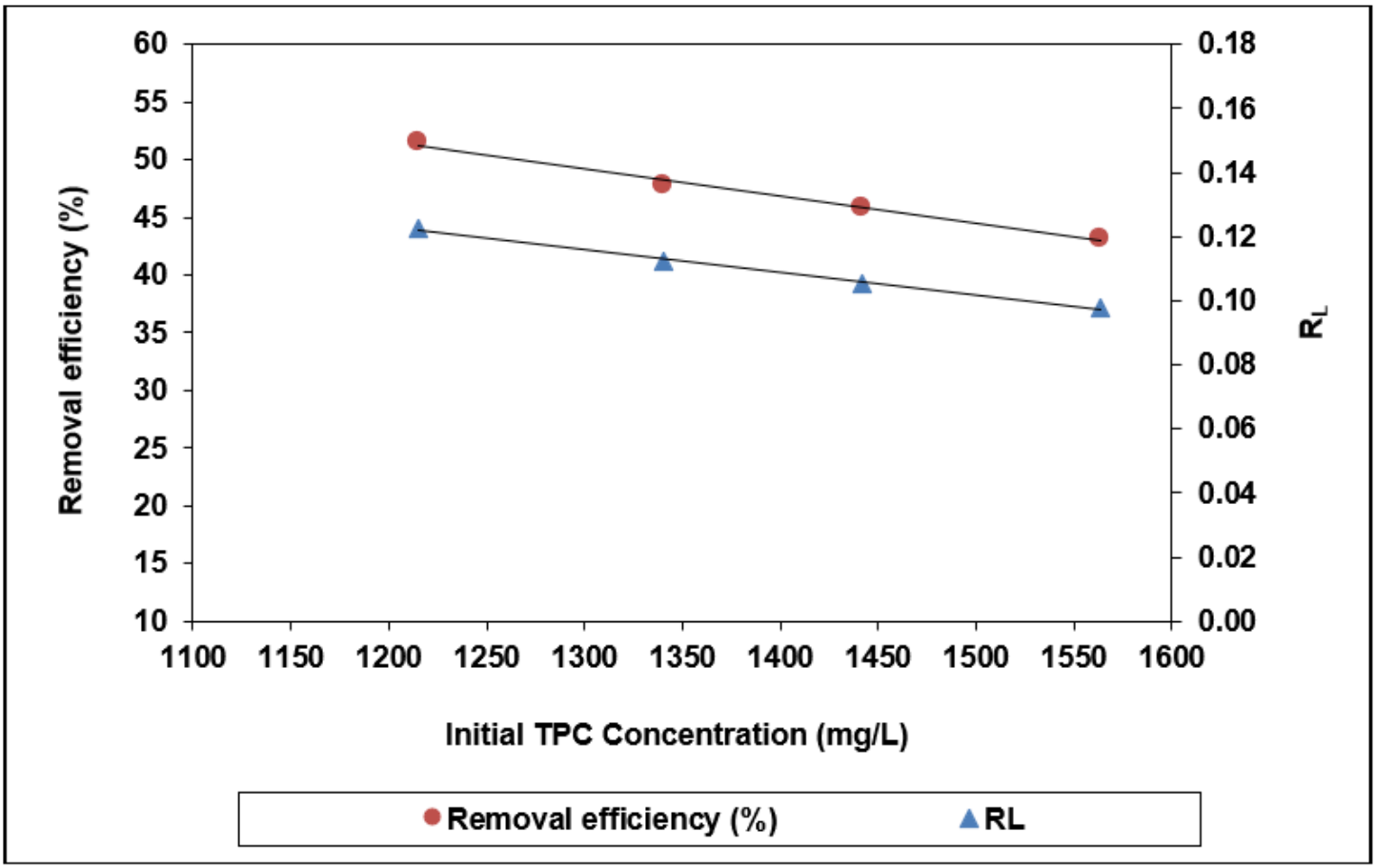


Figure 7

Effect of initial TPCs concentration on the percentage uptake using 1.0 g of PK-HCl, 10 mL of OMW, and constant temperature 303 K.

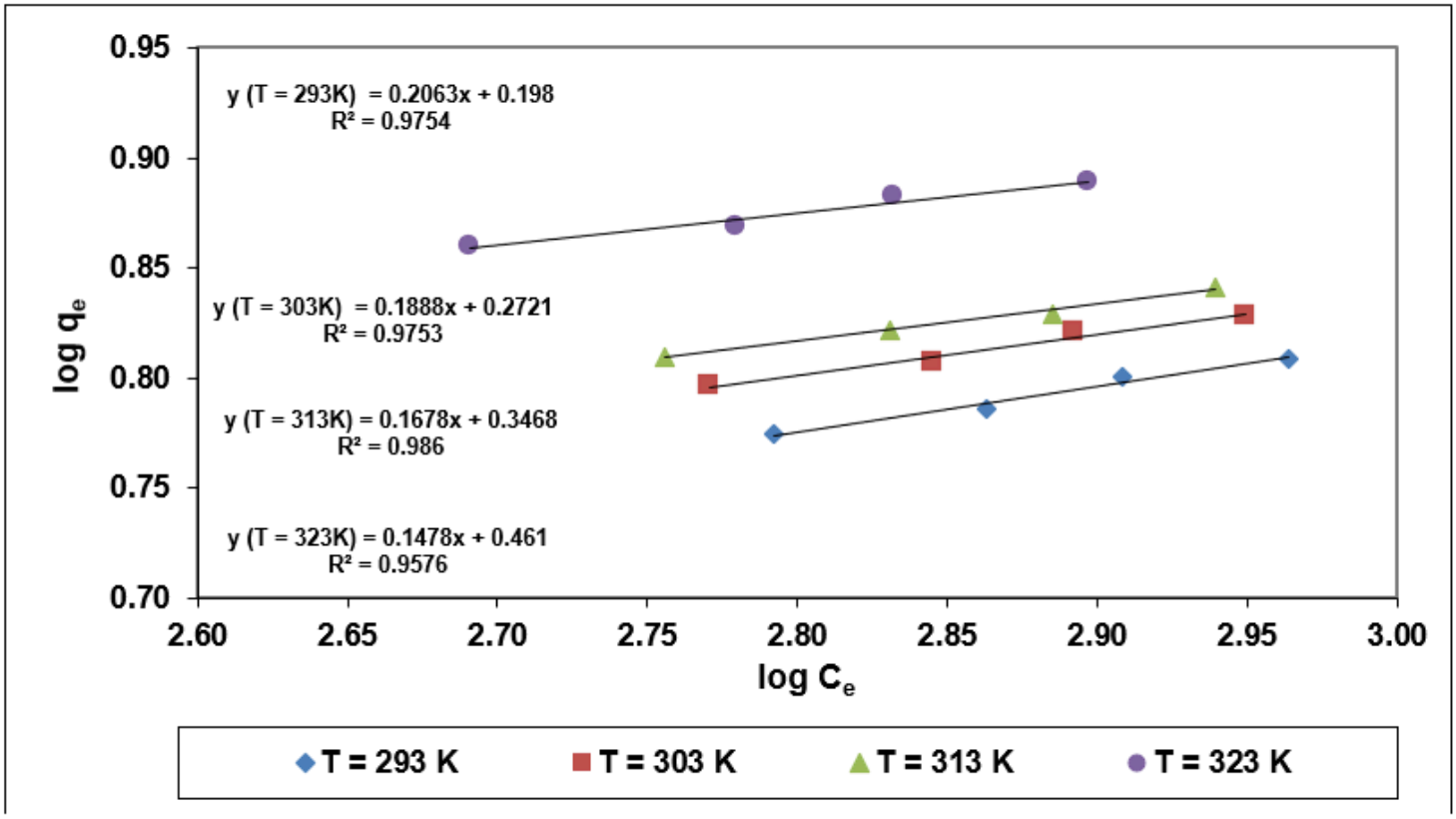


Figure 8

Freundlich isotherm for the adsorption of TPCs using PK-HCl. Experimental conditions were initial TPCs concentration 1340.6 mg/L, 1.0 g of PK-HCl, temperature = 293, 303, 313, and 323 K, 10 mL of OMW, contact time 4 hours, pH=6.

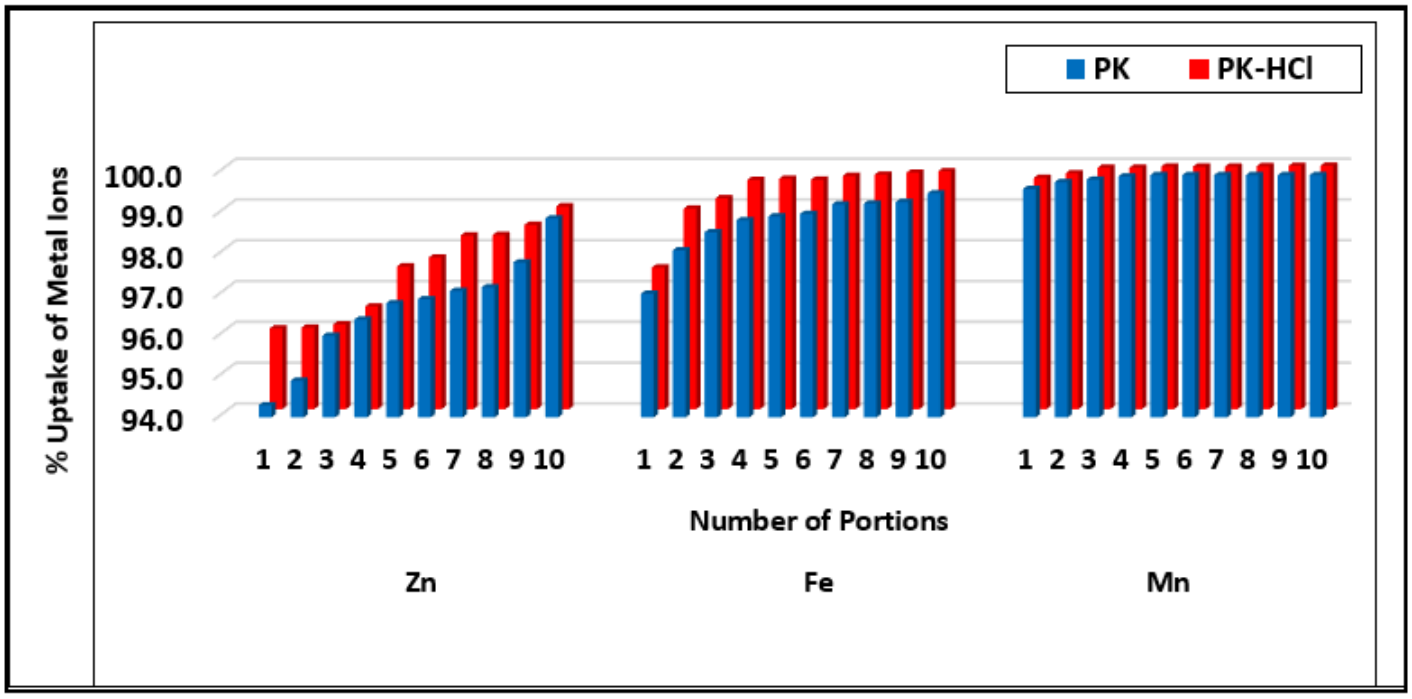


Figure 9

Percentage uptake of metal ions; Zn, Fe, Mn by PK and PK-HCl using column technique.